Particuology 58 (2021) 35–47

Contents lists available at ScienceDirect

Particuology

journal homepage: www.elsevier.com/locate/partic

Single droplet drying of detergents: Experimentation and modelling

Borja Hernandez[a,b], Rosa Mondragon[c], Mark A. Pinto[a], Leonor Hernandez[c], J. Enrique Julia[c], Juan Carlos Jarque[d], Sergio Chiva[c], Mariano Martin[b,*]

[a] Newcastle Innovation Centre, Procter & Gamble R&D, Newcastle upon Tyne, UK
[b] Departamento de Ingenieria Quimica y Textil. Universidad de Salamanca, Salamanca, Spain
[c] Departamento de Ingenieria Mecanica y Construccion, Universitat Jaume I, Castellon de la Plana, Spain
[d] Instituto de Tecnologia Ceramica, Universitat Jaume I, Castellon de la Plana, Spain

ARTICLE INFO

Article history:
Received 23 July 2020
Received in revised form 8 October 2020
Accepted 22 January 2021
Available online 3 March 2021

Keywords:
Drying
Single droplet
Acoustic levitator
Detergents

ABSTRACT

This study evaluates the single droplet drying (SDD) of detergents. Experimental data are used to validate a theoretical multistage model. The experiments are carried out in an acoustic levitator analysing six different detergent formulations at 393 K. The work is completed by developing a model based on conservation equations. The model is composed of the three stages observed in the drying curve. In the first stage, an external surface drying stage occurs until the surface is saturated and the crust is formed. In the next stage, the drying rate is governed by diffusion through the pores. At the same time, the particle heats up until boiling conditions are achieved in the core of the particle. At this point, the third stage begins. In the final stage, the droplet core is in boiling conditions which are governed by the pressure drop through the crust and the concentration of salts. This model has been evaluated for the different formulations being flexible to predict the drying of different mixtures with good accuracy.

Introduction

Many particulate products such as pharmaceuticals, foodstuffs (milk powder, instant coffee, etc.) and powder detergents are manufactured by spray drying (Masters, 1992). Spray drying works by contacting an atomized slurry with hot air in a chamber. The operation is a complex process that includes aspects from many areas such as fluid mechanics, heat and mass transfer, particle technology and reaction engineering. The understanding of these phenomena is critical for scaling-up and optimizing the production of the particles (Langrish, 2009; Masters, 1992; Woo, 2017). The use of validated computational models has helped in these areas by reducing the cost and time involved in experimental trials. The first models were based on heat and mass balances, involving assumptions such as uniform gas conditions and perfect-mixing inside the dryer (Strumillo & Kudra, 1986). The improvement in computational capabilities and the rapid expansion of the interest in spray drying has led to the development of more complex models in the last three decades (Langrish, 2009; Mujumdar & Huang, 2007). One of the most recurrent technologies in this area is computational fluid dynamics (CFD) (Harvie, Langrish, & Fletcher, 2002; Jaskulski, Zbicinski, & Wawrzyniak, 2015; Woo, 2017; Zbicinski, 2017). CFD models developed for spray drying towers are structured in different blocks such as airflow modelling, discrete phase momentum modelling, drying or particle quality (Hernández, Fraser, Martin de Juan, & Martin, 2018; Jaskulski et al., 2015; Woo, 2017). The modelling of the particles within the dryer has traditionally been performed by means of a discrete particle method that assumes a low concentration of particles. This allows the scale-up of the drying phenomena by studying the single droplet drying (SDD) of the material processed in the system. A range of approaches has been used to model SDD. Langrish (2009) recently classified the most popular approaches in four groups: The use of characteristic drying curves (CDC) (Langrish & Kockel, 2001; Zbicinski & Li, 2006), shortcut models based on the diffusion equation (Adhikari, Howes, Bhandari, & Troung, 2003; Kieviet, 1997; Liou & Bruin, 1981), receding-plane type of models that include diffusion and convection mechanisms (Chen et al., 1997; Keey & Suzuki, 1974; Seydel, Sengespeick, Blomer, & Bertling, 2004) and reaction engineering approaches (REA) (Chen & Xie, 1997; Lin & Chen, 2005). Apart from these types used in CFD, a more detailed approach based on population balances has also been developed for the description of the particle formation (Handscomb, Kraft, & Bayly, 2009; Mezhericher et al., 2012; Seydel, Blomer, & Bertling, 2004).

* Corresponding author.
E-mail address: mariano.m3@usal.es (M. Martin).

https://doi.org/10.1016/j.partic.2021.01.012

Nomenclature

Symbols

A	area, m^2
A_o	pressure amplitude of acoustic wave, Pa
$ANTA$	antoine correlation constant A
$ANTB$	antoine correlation constant B
$ANTC$	antoine correlation constant C
$ANTD$	antoine correlation constant D
B	particle velocity amplitude in the acoustic wave, m/s
C	concentration, kg/m^3
C_p	specific heat capacity, J/(kg K)
c_o	gas sound velocity, m/s
D	diffusivity, m^2/s
f_{lev}	oscillation frequency of the levitator, Hz
h	heat transfer convective coefficient, $W/(K\ m^2)$
H	moisture content of the droplet, %
K	mass transfer coefficient, m/s
k	thermal conductivity, W/Km
L_H	vaporization enthalpy, J/kg
m	mass, kg
Mw	molecular weight
Nu	Nusselt number
P	pressure, Pa
R	absolute radio, m
Sh	Sherwood number
T	temperature, K
t	time, s
w	mass fraction
y	droplet position, m
x	molar fraction
α_o	thermal diffusivity, m^2/s
γ	activity coefficient, kg/m^3
δ	crust length, m
ε	porosity.
ρ	density, kg/m^3
τ	tortuosity of the crust
ω	angular velocity, s^{-1}

Super-index

o	saturation conditions

Sub-index

1	1st drying period in experiments
2	2nd drying period in experiments
12	end of first period of drying
21	beginning of second period of drying
22	end of second period of drying
ac	referred to the acoustic levitator
bo	boiling at atmospheric conditions
c	critical
cs	cross-sectional
cr	crust
d	droplet
dm	dried matter
eq	equilibrium
l	liquid
o	initial conditions
sat	saturation
solid	solid phase
$t1$	instant 1
$t2$	instant 2
v	vapour
w	water
$\propto$	air

The CDC approach has been used in many works for modelling drying in spray dryers due to its simplicity (Langrish & Kockel, 2001; Woo et al., 2008; Zbicinski & Li, 2006). This type of model is semi-empirical and is represented by a set of simplified equations allowing fast computations with good predictions for small particle sizes (Keey, 1992; Mezhericher, Levy, & Borde, 2010) and industrial units. In this type of model, a first stage is simplified by analogy with evaporation of a small pure liquid droplet and a second stage shows a falling rate that is dependent on the critical, equilibrium and current moisture content values (Mezhericher et al., 2010). Similarly, the reaction engineering approach developed by Chen and Xie (1997) also uses simplified semi-empirical correlations for the modelling of SDD. This approach resembles the drying of the droplet by a kinetic model where the evaporation of water is an activation process having to overcome an energy barrier, whereas condensation or adsorption is assumed not to have an energy barrier (Lin & Chen, 2005). The application of this type of model is limited by the experimental characterization of the material since the activation energy and drying constant need to be estimated for each material under different moisture contents (Woo et al., 2008). However, this has not stopped REA from being applied to different droplet materials such as milk droplets (Lin & Chen, 2005) and maltodextrin (Lin & Chen, 2002; Patel, Chen, Lin, & Adhikari, 2009; Chen and Putranto, 2013). Small differences of around 5% between this approach and the CDC are found when comparing both (Woo et al., 2008).

Contrary to the simplicity of the two previous approaches, deterministic models based on mass, momentum, and energy conservation equations provide a more detailed explanation of the phenomena involved and, in some cases, the droplet structure. As with the two previous types, these models are based on the characterization of the transport of water in the boundary layers of spherical droplets as proposed by Ranz and Marshall (1952a, 1952b). These studies, which assumed infinite thermal conductivity in the droplet, were extended in the study of Abramzon and Sirignano (1989), who suggested the use of an effective thermal conductivity for the liquid of the droplet to improve the prediction of the drying rate. Another first principles-based model that modifies the drying rate as a function of the droplet properties was proposed by Nesic and Vodnik (1991). This model includes the shrinkage of the droplet and the formation of a crust so that water diffusion is affected by its thickness. If the pores created in that crust have lower effective diffusion coefficient than the water in the boundary layer, the global diffusion coefficient decreases (Nesic & Vodnik, 1991). These first principles-based models assume a uniform temperature for the entire droplet. Newer models have been developed to include the temperature distribution for some specific cases. In the case where Biot and Lewis numbers were very low and droplet temperatures were below the boiling temperature, Farid (2003) developed a model that includes the temperature distribution within the droplet. A model considering the temperature distribution, the influence of the concentration and the formation of the crust was recently developed by Darvan and Sommerfeld (2014). In addition to defining a new model, their study provided more accurate predictions in the stage transitions for milk droplets.

All these previous models mainly focused on milk droplets evaluated at low temperatures. A few studies such as the ones performed by Sano and Keey (1982) and Mezhericher, Levy, and Borde (2008) have used temperatures above the boiling temperature of water for the SDD of milk. In both cases, higher temperatures were only observed at the end of the drying curve without showing boiling phenomena within the droplet. One of the first works including boiling in drying was developed by Hecht and King (2000) for sucrose droplets. Their work proposed a model for boiling based on the energy balance and a correlation for the boiling temperature as a function of the moisture content in the droplet. Apart from the

focus on boiling, previous works also focused on the crust behaviour observing that it could be deformed at high temperatures depending on the flexibility and capillarity forces. In a recent work, Tran, Jaskulski, Avila-Acevedo, and Tsotsas (2017) studied this deformation observing the rupture of milk particles for temperatures above 413 K and proposed a model to estimate the final diameter and drying rates of such droplets.

Even though boiling rarely takes place in the production of milk powders since denaturalization of the proteins appears at 345 K (Dannenberg & Kessler, 1988), the study of Tran et al. (2017) provides relevant description of drying at high temperature and it is relevant to more stable materials such as detergents and ceramics that are processed at high temperatures. Focusing on the drying of detergent droplets, two studies have developed SDD models for their implementeation within the CFD modelling of spray drying towers. Jaskulski, Wawrzyniak, and Zbicinski (2016) proposed a CDC model. The model was validated using the temperature distribution within the tower and was applied to predict agglomeration. The second study by Ali et al. (2017) used a variation based on experimental fittings of the model of Hecht and King (2000). In these two studies the drying curves were not validated either for different formulations or with direct analysis of the drying of the droplet. In particular, in the work of Ali et al. (2017) the Hecht and King's model, initially developed and validated for the drying of sucrose powders (Hecht & King, 2000), was used but not validated for the direct analysis of single droplets of detergent. In that work, the drying model was straightforward defined from the characterization of the properties without considering the evaluation at single droplet drying level. Furthermore, a diffusion stage in the crust was empirically modelled without any physical background. Thus, this work aims to provide an intermediate study at single droplet level evaluating the influence that the crust may play on the drying of droplets and using a physical based model when the drying is governed by the diffusion through the crust. Since the model is then desired to be implemented into CFD codes, the aim is not to develop a very complex model such as the ones based on population balances. The work focuses on characterizing each formulation with a different diffusion coefficient, which is affected by the composition of the detergent formulation. Therefore, this work also provides a comparison of the SDD of different detergent formulations.

The rest of the paper is structured as follows. In section "Experimental methodology", the experimental methodology consisting on the use of a levitator is presented. In section "Modelling approach", the theoretical model based on experimental observations is developed. In section "Experimental results and model validation", the experimental results are presented together with the evaluation of the model. Conclusions are presented in section "Conclusions".

Experimental methodology

Experimental apparatus

The study of drying kinetics of particles can be performed using different methods such as a conventional microbalance, a balance in combination with a drying tunnel, an acoustic levitator, a magnetic suspension balance or by glass filament (Tsotsas & Mujumdar, 2009). Previous works have also shown the application of some of these techniques to the characterization of single droplet drying at elevated temperatures. For example, Mondragon et al. (2011) and Tran et al. (2017) used a non-intrusive method such as acoustic levitator but that does not allow to predict the particle temperature, or Ebrahim (2019) used a microbalance that allows the prediction of the temperature but it slightly modifies the structure of it. In this work the acoustic levitator is used. This technique was introduced by Yarin, Brenn, Kastner, Rensink, and Tropea (1999) for the evaporation of droplets and for the first time it was used for studying the drying of droplets with suspended solids by Groenewold, Möser, Groenewold, and Tsotsas (2002). In this work, the system used composed of three systems as presented in Fig. 1: the acoustic levitator itself consisting of an ultrasonic 58 kHz horn and a concave reflector; an optical system consisting of a white light source with a CCD camera; and an air conditioning system.

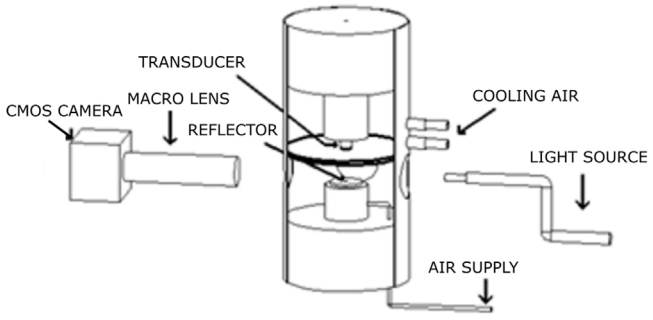

Fig. 1. Ultra-sonic levitator used for the experiments.

The levitator has been modified to be used with higher temperatures, up to 423 K, than the initial specifications allowed by the supplier, 333 K. Previous works that used this modified levitator reported stability for the drying of multiphase droplets at 393 K (Mondragon et al., 2011; Yarin, Brenn, Kastner, & Tropea, 2002). The modification has been performed as presented in Fig. 2. Two metallic chambers separated by the insulator can be found. The first is identified as the "cold chamber" and contains the ultrasonic transducer of the levitator. The temperature of this chamber cannot be higher than 333 K to prevent damage to the piezoelectric transducer. This temperature is controlled by forced convection using a flow of cold air. The second "hot chamber" contains the lower part of the levitator. The temperature of this chamber is controlled by an electric heater, see Fig. 2. The ultra-sonic levitator uses an air stream that enters the levitator tube through an array of holes located in the reflector (Mondragon et al., 2011).

The air conditioning system is composed of a dierite air-drying cartridge, two-mass flow controllers and an evaporator/mixer unit. This system allows temperatures up to 473 K and humidity up to a dew point of 353 K. To prevent the cooling down of the air stream from the conditioning system to the levitator, the tube that connects both devices, as well as the reflector, needs to be heated using electric heaters.

A CMOS camera with a back-light illumination is used to measure the droplet cross sectional area and the vertical position of the droplet during the drying process. A resolution of 500 pixels/mm and a recording speed of 87 fps are set for all experimental conditions. The recorded images are analyzed later to determine the drying curve.

Experimental procedure

In this study, six formulations have been analyzed. The formulation of these detergents is complex involving different species such as crystalline and amorphous salts, polymers, surfactants and water (Griffith, Bayly, & Johns, 2008). Each formulation has been analyzed several times but high instabilities are obtained due to the droplet oscillations. Examples of Formulation A and B for the cases with lowest oscillations are reported in Figs. S1 and S2 of the supplementary material. From these cases, the one with lowest dispersion is used in the evaluation of the model presented in the following chapters. The droplets are introduced with a syringe into the hot chamber of the levitator. The droplet size selected for the

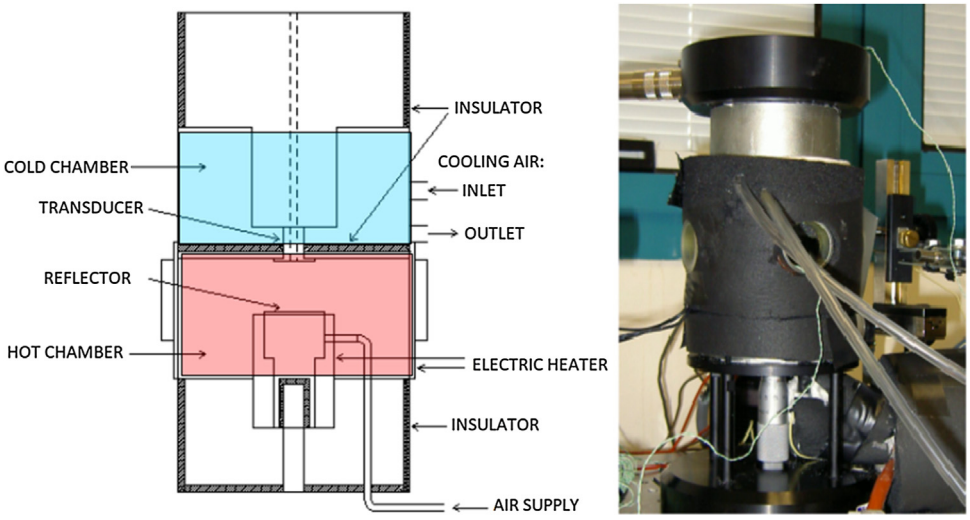

Fig. 2. Modified acoustic levitator used for the experiments.

study is around 800 μm in diameter. The exact size is captured by the camera to avoid errors in the modelling part of this work.

The flow rate and temperature of the air stream are set to 0.5 l/min and 393 K, above the boiling temperature of the formulations at atmospheric conditions (between 368 K and 381 K), to ensure constant drying conditions around the droplet, to ventilate the acoustically induced vortex system around the droplet from liquid vapour and to avoid the blow out of the droplet (Mondragon et al., 2011; Yarin et al., 2002). The estimated flow velocity at the droplet based on the analysis from Yarin et al. (1999) was 0.7 cm/s. The drying air is introduced in the levitator hot chamber after flowing through the drierite air-drying cartridge to remove the initial moisture content and to minimize relative humidity for the drying tests.

The drying of the droplet is recorded by the CMOS camera. The images reported are subsequently analyzed by Matlab®'s Image Processing Toolbox, which reports the particle cross-sectional area of the droplet and the position of the droplet.

Modelling approach

Historically, the modelling of particle drying in CFD simulations for spray drying towers has been performed using one of the 4 theoretical approaches presented in the introduction. In this study a first-principle based model including diffusion and convection mechanisms is developed. The mechanism and the equations used to model them are discussed in this section.

Theoretical description of the model

The drying mechanism described in Fig. 3 is used. It is composed of the following three stages:

- A surface drying stage where the surface water diffuses into the surrounding air and results in a shrinkage of the droplet. This stage occurs until the locking point is achieved. At this point, the surface is dry and the generation of the crust begins.
- In the second stage drying is governed by the diffusive resistance of water through the pores formed in the crust that grows from the surface to the centre of the droplet. Apart from controlling the diffusive mass transfer, the crust is also assumed to govern the transition to boiling. The droplet heats up until it reaches boiling conditions. This happens when the vapour pressure within the droplet is equal to the pressure in the wet core, is the latter given by the atmospheric pressure plus the pressure drop through the crust.
- Once the boiling conditions are achieved in the wet core, the drying rate increases by vapour convection through the pores. Since the evaporation rate within the droplet increases due to boiling, the flow through the pores also suffers an increase and the droplet behaves as a "pressure cooker" where the pores are the "valve" that control the internal pressure. Apart from the change in the drying rate, it is also important to remark the influence of the nucleation regime expected for boiling. In the extreme case, where the crust reaches the gas temperature quickly, the maximum difference between the boiling temperature of the core (373 K at atmospheric conditions) and the temperature of the crust (temperature of 393 K in the air) is never higher than 20 K. In practice, smaller temperature differences are generated because (1) the salts dissolved in the core increase the boiling temperature and (2) because the crust presents a pressure drop, allowing higher boiling temperatures to be achieved inside the core. These two effects combined result in a smaller temperature difference between the boiling conditions and the crust. Since this difference is small, it is assumed that the boiling regime does not generate stable bubbles (Incropera, Dewitt, & Bergman, 2006), see Fig. S1 in the supplementary material. As a result, the pressure within the droplet is not higher than the rupture strength of the material and the droplet does not result in bursting. The pores can maintain their shape or they can only suffer a plastic deformation by the pressure increasing their size. The characterization of these pores is extremely challenging during drying and the only concern observed is that bursting does not occur as presented in the videos attached as supplementary material. Therefore, the modelling of this third stage is carried out dividing the third stage is two parts:
- A first sub-stage where the boiling is governed by the pressure drop through the pores. The pores formed in the previous stage still present a resistance, maintaining the boiling temperature at higher conditions than the boiling temperature at atmospheric conditions.
- A second sub-stage where the boiling temperature is governed by the moisture content of the droplet. In this second stage, the concentration of solids in the core increases. This results in a decrease in the activity coefficient and an increase in the boiling temperature, increasing the likelihood that equilibrium is eventually reached. This stage is assumed to last until the final equilibrium moisture content is achieved.

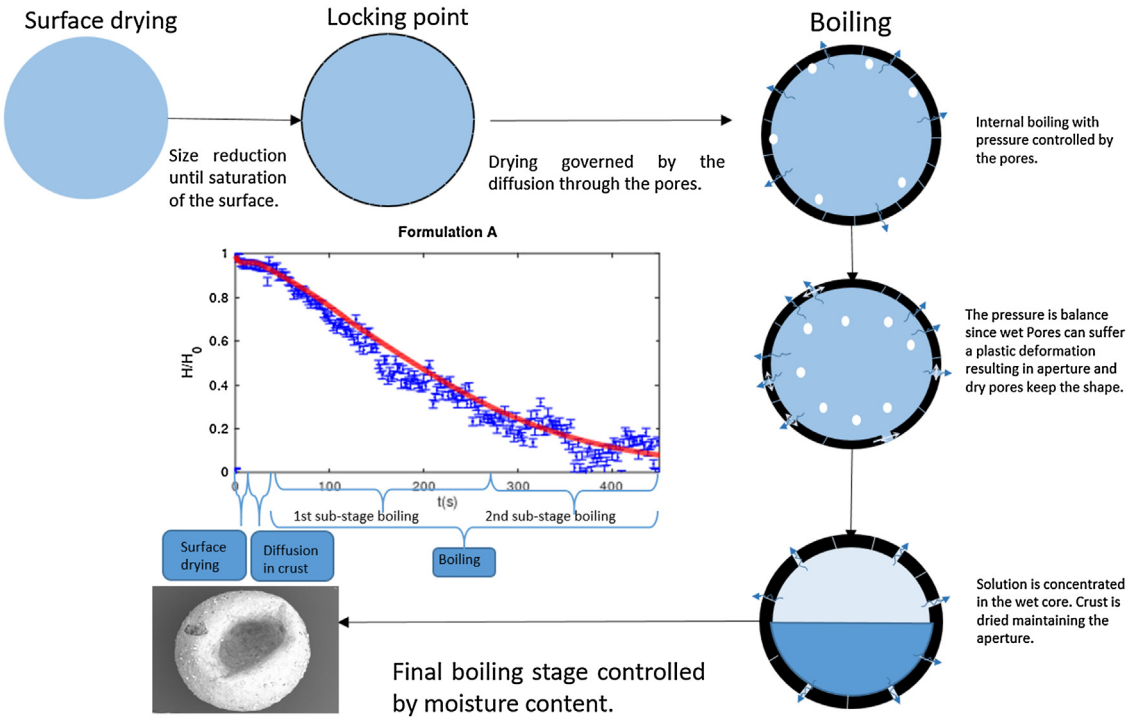

Fig. 3. Droplet drying mechanism.

Mathematical modelling

The model has been developed in gProms®, ModelBuilder® v.5.1 and the stages previously described are modelled as presented in the following paragraphs.

Modelling of the 1st drying stage

The first stage is modelled with the equations presented below. The mass balance for the drying of the droplet during this stage is modelled with Eq. (1), which corresponds to a system controlled by mass transfer through a boundary layer.

$$\frac{dm}{dt} = 4\pi R^2 \cdot K \cdot \frac{(P_{v,s} - P_{v,\infty})MW_w}{RT} \tag{1}$$

In Eq. (1), P_v is the vapour pressure. The subscript s refers to the droplet-air interface and the subscript ∞ refers to the air-bulk phase. The vapour pressure is computed by Eq. (2) as a function of the moisture concentration in the droplet, C_1, the activity coefficient, γ_1, and the saturation pressure of the vapour, P_1^0. The activity coefficient, γ_1, is modelled using an empirical Eq. (3) as a function of the moisture content. The parameters in Eq. (3) are experimentally determined from the desorption isotherm of each formulation at 323 K. The saturation pressure is computed by also the empirical Eq. (4).

$$P_{v,s} = x_v \cdot \gamma_l \cdot P_l^0 \tag{2}$$

$$\gamma_l = a \cdot C_l^b \left[\frac{\text{kg}}{\text{m}^3}\right] \tag{3}$$

$$P_l^0\,[\text{Pa}] = 10^{8.07131 - \frac{1730.63}{T_d[\text{K}] - 28.515}} \cdot \left(\frac{1.01325 \cdot 10^{-5}}{760}\right) \tag{4}$$

The mass transfer coefficient, K, in Eq. (1) is computed using Eq. (5) as a function of the particle radius, R, the mass diffusivity, D_w, and the Sherwood number for acoustically driven levitation, Sh_{ac}.

$$K = \frac{Sh_{ac} \cdot D_w}{2R} \tag{5}$$

The water-air diffusivity is computed using the empirical Eq. (6) (Mezhericher et al., 2008).

$$D_w = 3.564 \cdot 10^{-10} \cdot (T_d\,[\text{K}] + T_\infty\,[\text{K}])^{1.75} \tag{6}$$

The Sherwood number, Sh_{ac}, is computed using Eq. (7) as reported by Yarin et al. (2002).

$$Sh_{ac} = \left(\frac{45}{4\pi}\right) \cdot \frac{B}{(\omega D_w)^{1/2}} \tag{7}$$

Where the angular velocity, ω, is determined from the oscillation frequency of the levitator (f_{lev}) by Eq. (8). The gas-particle velocity amplitude in the acoustic wave, B, is computed using Eq. (9). In Eq. (9), ρ_∞ is the density of the air at 393 K, c_o is the gas sound velocity, which takes a value of 397 m/s at 393 K, and A_o is the effective pressure amplitude of the acoustic field. The value of the pressure amplitude of the acoustic field is a parameter determined with the first formulation and subsequently used in the remaining experiments. The value obtained for A_o from the first experiment is 1.2×10^3 Pa. This value finally results in a Sherwood number between 2.3 and 2.6, within the range reported by Yarin et al. (2002).

$$\omega = 2 \cdot \pi \cdot f_{lev} \tag{8}$$

$$B = \frac{A_o}{\rho_\infty c_o} \tag{9}$$

In the same way, a heat balance is also performed during this stage as presented in Eq. (10).

$$\frac{dT}{dt} = \frac{1}{m\left(C_s C_{ps} + C_l C_{pl}\right)}\left[4\pi R^2 \cdot h \cdot (T_\infty - T_s) + L_H \frac{dm}{dt}\right] \tag{10}$$

The heat transfer coefficient through the boundary layer, h, is computed using Eq. (11) as a function of the Nusselt number for acoustically driven levitation, Nu_{ac}, and the thermal conductivity of the air, k_{air}. The Nusselt number for acoustically driven levitation

Table 1
Variables defined for the modelling.

Variable	Value
L_H (J/kg)	2,264,760
C_{psolid} (J/kg K) [40]	700
C_{pl} (J/kg)	4185
$k_{air(393\ K)}$ (W/m K)	0.033
$\alpha_{o(393\ K)}$ (m^2/s)	3.75×10^{-5}

is determined from the thermal diffusivity of the air, α_o, and the Sherwood number as presented in Eq. (12).

$$h = \frac{k_{air} \cdot Nu_{ac}}{2R} \tag{11}$$

$$Nu_{ac} = \left(\frac{D_w}{\alpha_o}\right)^{\frac{1}{2}} Sh_{ac} \tag{12}$$

Apart from the parameters defined in the previous equations, the rest of parameters have been assumed to be constant with the values presented in Table 1.

Modelling of the 2nd drying stage

The second stage begins with the locking point, which is achieved when the droplet surface gets dried and the crust starts to be generated. This locking point is defined as a function of a critical moisture content, C_{lcr}, This is a parameter in the drying curve determined for each formulation. After achieving the locking point, the crust grows and presents a resistance to mass transfer. Despite the low porosity of the particle, the diameter of the pores is assumed to be much greater than the vapour molecular free path. As a result, the Knudsen number is much smaller than unity (Minoshima, Matsushima, Liang, & Shinohara, 2002) and the overall mass transfer rate is computed as the sum of two resistances as defined in Eq. (13). In the denominator of Eq. (13), the first term corresponds to the resistance due to the diffusion across the boundary layer, which is obtained from Eq. (5), and the second term is the resistance given by the diffusion through the crust. R_c is the droplet radius that remains constant once the crust has been formed. Sh_{ac} is computed as presented in Eq. (7) and D_w is the diffusivity of water in air. In the second term, D_{cr} is the diffusion coefficient across the crust pores and δ is the crust thickness, which grows as presented in Eq. (14). In Eq. (14) the crust thickness is shown to be dependent on its porosity, ε. This porosity is covered by the vapour generated from the core with a flow rate that can be computed using Eq. (15).

$$\frac{dm}{dt} = \frac{MW_w}{RT} \cdot \frac{2\pi\left(P_{v,s} - P_{v,\infty}\right)}{\frac{1}{R_c Sh_{ac} D_w} + \frac{\delta}{2D_{cr}R_c(R_c-\delta)}} \tag{13}$$

$$\frac{d\delta}{dt} = \frac{1}{(1-\varepsilon)\cdot\rho_{solid}\cdot 4\cdot\pi\cdot R_C^2}\frac{dm}{dt} \tag{14}$$

$$\left(\frac{dm}{dt}\right)_d = \frac{dm}{dt}\frac{\varepsilon\cdot\rho_v}{(1-\varepsilon)\rho_d} \tag{15}$$

A heat balance is also formulated on the droplet core as presented in Eq. (16). The resistance to the heat transfer into the droplet is defined in the denominator of the first term in brackets. It represents the resistance to the heat transfer in the boundary layer and the resistance in the crust. The second term within the brackets corresponds to the energy consumed to evaporate the solvent. The third term is the vapour required to cover the pore of the crust. The fourth term is the energy absorbed by the crust, which is assumed to be heated until it achieves the external gas temperature.

$$\frac{dT}{dt} = \frac{1}{\left(m_{s_{core}}C_{p\,solid} + m_l C_{pl}\right)}\left[\frac{2\pi R_c Nu_{ac}k_{air}\left(T_\infty - T\right)}{1+\frac{Nu_{ac}k_{cr}}{2k_{cr}}\frac{\delta}{R_c-\delta}} + L_H\frac{dm}{dt} + L_H\left(\frac{dm}{dt}\right)_p - m_{s\,cr}C_{p\,solid}\left(T_\infty - T\right)\right] \tag{16}$$

In addition to the critical moisture content, C_{1cr}, the diffusivity through the crust is estimated from SDD experiments. The remaining parameters involved in this second stage have been defined in Table 1, except for the thermal conductivity of the crust, which is assumed to be 0.7 W/mK (Konior czyk & Konca, 2013), the conductivity of the main dried component (Griffith et al., 2008).

In defining the transition to the third stage, it is assumed that there is a vapour-liquid equilibrium within the droplet given by Eq. (17). Boiling conditions in the wet core are achieved when the saturation pressure of the vapour in this equilibrium is equal to the pressure within the core. The pressure within the core is computed as the sum of the atmospheric pressure and the pressure drop across the crust, which is obtained from the Carman-Kozeny equation, Eq. (18). In this equation, the viscosity of the steam, μ, is taken to be 1.4×10^{-5} Pa s, the superficial velocity, v_{cs}, is computed from the drying rate as presented in Eq. (19), the mean diameter of the particles that compose the crust, d_{mpc}, is assumed to be 1 μm, and the porosity of the crust, ε, is a parameter to be determined. The pressure at the end at which transition occurs is also given as a free parameter to be characterized for every formulation.

$$P_{wc} = P_{atm} + \int_{\delta=0}^{\delta=\delta}\frac{\partial P_{cr}}{\partial\delta} \tag{17}$$

$$\frac{\partial P_{cr}}{\partial\delta} = -\frac{180\mu}{d_{mpc}^2}\frac{(1-\varepsilon)^2}{\varepsilon^3}v_{cs} \tag{18}$$

$$\frac{dm}{dt} = v_{cs}\cdot\rho_v\cdot 4\cdot\pi\cdot R_c^2 \tag{19}$$

Modelling of the 3rd drying stage

In this stage of the drying of the droplet, a hollow core is assumed to be formed. The drying rate is controlled by two mechanisms: First, an equilibrium between the heat and mass transfer is achieved. Water activity in the core is 1 and the pressure in the core, which is also influenced by the pressure drop across the crust, is equal to the vapour pressure defined by the Antoine equation for water. As a result, the temperature in the droplet core, where boiling occurs, is constant. Thus, due to the equilibrium reached at boiling, during this period the drying rate of the droplet is computed from the energy balance, Eq. (20) and the temperature is assumed to be constant, see Eq. (21).

$$\frac{dm}{dt} = \frac{hA_d\left(T_\infty - T_p\right)}{L_H\cdot\left(1+\frac{\rho_v}{\rho_{wc}}\right)} \tag{20}$$

$$\frac{dT}{dt} = 0 \tag{21}$$

This first period of the third stage lasts until a critical moisture content is achieved. Below this critical moisture content, the solids concentration in the droplet core reduces the activity of the water and part of the energy provided to the droplet is retained. Therefore, mass transfer in this stage is characterized by multiple equilibria between mass and heat transfer that follows the boiling temperature equation, Eq. (22), corresponding to the composition at the core. Apart from this equation, the energy balance is computed by Eq. (23) (Hecht & King, 2000). One way to determine the boiling temperature as a function of the moisture content, Eq. (22), was provided by Ali et al. (2017). They used a modified Antoine correlation as presented in Eq. (22). However, the values of the factors used in Eq. (23) change for every formulation.

$$T_d\,[K] = \exp\left(\frac{ANTA}{ANTB + ANTC\cdot w_l} - ANTD\right) + T_{bo}\,[K] \tag{22}$$

Table 2
Parameters of the model.

Parameters to be fitted in the model
C_{1cr} (Critical moisture content for transition from first to second stage
A_o (Amplitude of the acoustic field, only characterized once and re-applied to the remaining droplets)
D_{cr} (Diffusion coefficient of the crust)
ε (Porosity of the crust)
Pressure in the transition from second to third stage
Coefficients for boiling: *ANTA*, *ANTB*, *ANTC*, *ANTD* & T_{bo}

$$\frac{dm}{dt} = \frac{hA_d\left(T_\infty - T_p\right)}{\lambda * \left(1 + \frac{\rho_v}{\rho_{wc}}\right) - \left(w_{s_{core}} C_{ps} + w_l C_{pl}\right) C_s \frac{dT_d}{dC_l}} \tag{23}$$

Taking into account all the stages defined in the model, the following parameters defined in Table 2 are characterized in the model.

Experimental results and model validation

This section presents the experimental results in section "Experimental results" together with a validation of the model developed in this work in section "Model validation".

Experimental results

The analysis of measurements by Matlab®'s Image Processing Toolbox provides the projected area of the particle and its relative position. One example of these measurements is provided in Fig. 4 for formulation A. Data for the remaining formulations are presented in Fig. S4 to S9 of the supplementary material. They show the two following periods:

- A first period showing a shrinkage of the area together with a rapid increment of the relative position. In Fig. 4, this period corresponds to the first 20 s of drying.
- A second period where the cross-sectional area of the droplet remains constant and the relative position increases until the droplet reaches an equilibrium position.

During the first period, the shrinkage of the droplet is due to the evaporation of the moisture on the surface. In order to compute the mass transfer rates during this first period $\left(\frac{dm}{dt}\Big|_{1st}\right)$, d^2-law is applied (Kastner, Brenn, Rensink, & Tropea, 2000), as presented in Eq. (24). ρ_w is the density of the water, d_{t1} and d_{t2} are the diameters between two subsequent time-steps and t_{t1} and t_{t2} are the time between two time-steps.

$$\frac{dm}{dt}\Big|_{1st} = \frac{\pi}{6}\rho_w \frac{d_{t1}^3 - d_{t2}^3}{t_{t1} - t_{t2}} \tag{24}$$

The characterization of the drying rate after the locking point cannot be determined as presented in Eq. (24) since the droplet diameter remains constant. Two approaches have been proposed for this characterization: Groenewold et al. (2002) measured an indirect variable as it is the moisture content of the air at the exit of the levitator. Alternatively, Yarin et al. (2002) suggested the use of the change in the axial position since the vortices generated in the levitator chamber do not completely ensure the homogenization of the air moisture concentration. This can also have an impact on the prediction of the time at when transition between stages occur. Thus, the method proposed by Yarin et al. (2002) is followed. Based on this method, the mass of the droplet is computed by Eq. (25) (Kastner et al., 2000). In this equation, y_{21} and y_{22} are the droplet positions at the beginning and end of the second drying stage, respectively, $y(t)$ is the instantaneous position of the droplet, t is the time, which is subtracted from the time at the beginning of the second stage, t_{21}, and m_{21} is the liquid mass content in the droplet at the beginning of the second drying period, which is computed by Eq. (26):

$$\frac{dm}{dt}\Big|_{2nd} = \frac{m_{21}}{t - t_{21}} \frac{y(t) - y_{21}}{y_{22} - y_{21}} \tag{25}$$

$$m_{21} = \frac{\pi}{6} d_0^3 \rho_d \left(1 - w_{solid}\right) - \frac{\pi}{6}\rho_l \left(d_0^3 - d_{12}^3\right) \tag{26}$$

Table 3
Percentages of time per stage.

Formulation	1st stage (%)	2nd stage (%)	3rd stage (%)
A	6.4	25.6	68
B	6.9	16.5	76.6
C	1.8	15.3	82.9
D	8.6	4.3	87.1
E	11.2	2	86.8
F	5	14.4	80.6

As a result, a drying curve can be obtained from this analysis as presented by the blue dots in the plot of Fig. 5. In this Fig. 5 the blue dots correspond to the experiments and the red lines correspond to the results of the model presented in section "Modelling approach". The modelling results are described in the following section "Model validation". The experimental results of Fig. 5 show three stages: A short first stage where the moisture evaporates by diffusion, a second stage where the drying rate is reduced and a third stage that shows another increase in the drying rate. It is also observed from the analysis of the radius presented in Fig. S4 to S9 of the supplementary material that the droplet radius remains constant after the second stage has been reached. The surface of the droplet is dried and further drying only occurs for the moisture within the droplet. Thus, for the droplets studied in this work, the droplet radius can be determined fitting the transition from the first to the second stages in the drying curve. This second stage does not take a long time and it can be very short as in formulation E, see Fig. 5, which is the most similar to the one presented in the work of Griffith et al. (2008). In that work, only one detergent formulation was analyzed and drying was carried out at 355 K, below the boiling temperature. In order to quantify the length of this second stage, the percentage of time of each stage is shown in Table 3. The results show that the first stage corresponding to drying governed by diffusion, is the shortest. On the contrary, the third stage is the longest. In this stage, the drying is governed by boiling. Hence, most of the drying of the particles occurs during the third stage, while the structure of the droplet and its transition to having a dry surface occurs during the two first stages.

Another observation from the experimental results is that there are oscillations in the moisture content in some of the formulations. Looking at the drying curves for formulations B, E and F in Fig. 5, oscillations appear in the moisture content during the third stage. These oscillations can be explained by the heterogeneous drying of the droplet which results in a loss of sphericity in the droplet and makes the droplet rotate. The videos attached in the supplementary material show the drying of two formulations. In those videos, and from the drying curves, it can be observed that the rotation tends to increase (even causing the oscillation of the droplet) when the droplet is reaching its equilibrium moisture content. This fact is promoted by the distribution of material within the droplet when it is getting dried. As can be seen in Fig. 6, most of the material in the droplet is concentrated in the external crust of the droplets, which is unbalanced, and makes the droplet oscillate.

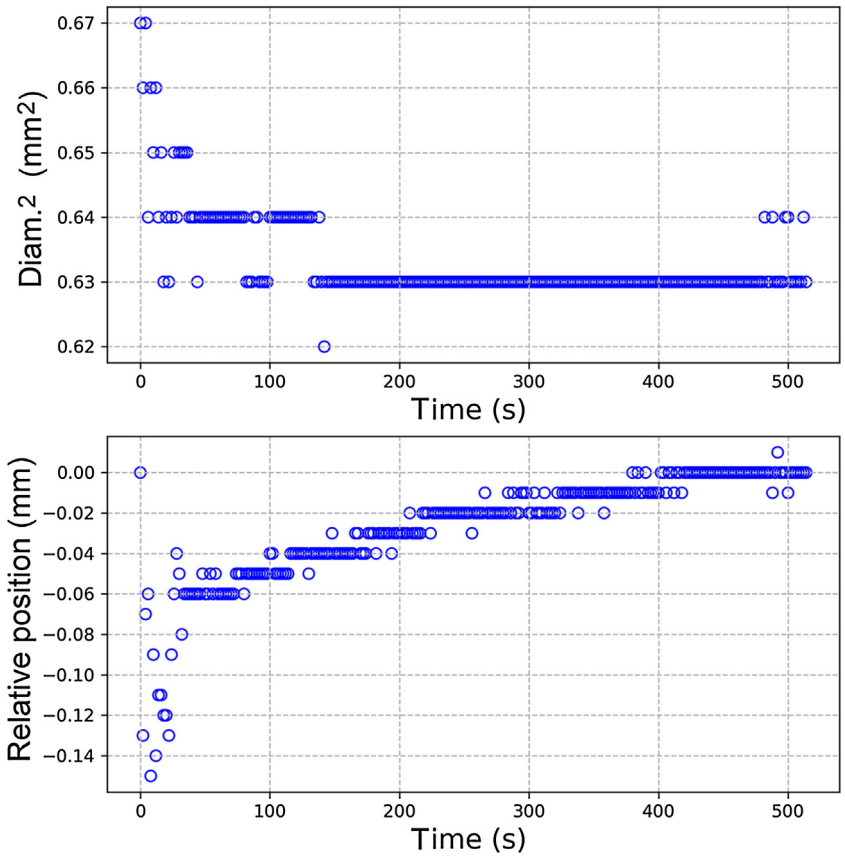

Fig. 4. Square diameter (top) and particle relative position (bottom) for the drying of a droplet of formulation A.

Model validation

In this section, the drying curves of the formulations are used to validate the model described in section "Modelling approach" against the experimental moisture content, radius and density.

Drying curves evaluation

The prediction of the moisture content is presented in Fig. 5. The model proposed accurately fits the moisture observed experimentally. Deviations are primarily due to the rotation of the droplet generated in the experiment, being more apparent in formulations B, E and F.

Analysing the prediction in each of the stages, the first stage is captured well for most of the formulations. The use of the Sherwood and Nusselt numbers based on the acoustic field reduces the error in the prediction as also observed by Yarin et al. (2002). For formulation F, small differences exist with the experimental data. The model estimates a higher drying rate than the one measured. However, these differences do not impact the estimation of the locking point as it is predicted well for all the formulations.

Analysing the second stage, the moisture content during this stage is predicted with reasonable accuracy for all the formulations. As previously mentioned, formulation B is the one that shows a poorer match with experimental data due to the oscillations of the droplet. The transition from this second stage to the third one is characterized by the pressure drop generated in the crust. The computed pressures inside of the droplet are presented in Table 4 for all the formulations. Even that they cannot be characterized since temperature in the core cannot be measured with this technique they are estimated to be higher. It can be seen that the pressure for the transition to boiling, determined from the crust porosity and thickness, tends to be higher for formulations with a longer second stage. However, formulation F shows a pressure of 1.42×10^5 Pa which is as high as the one achieved in formulations A and B. This pressure is obtained because the pressure for the transition to the third stage is determined as a parameter for each formulation. The parameter estimation does not only take into account the values of the second stage, but also considers the values from the third stage. As a result, the pressure obtained by the parameter estimation is also influenced by the experimental data of both stages. It is important to consider the data from the third stage in the parameter estimation because the pressure achieved at the end of the second stage is the same as the pressure at the beginning of the third stage where the drying rate is governed by the temperature difference between the droplet and the bulk. For example, if higher pressures had been achieved within the droplet during the second stage, the wet core would have had higher temperatures and the drying rate in boiling conditions would have been too small to predict the moisture content of the droplet. Thus, the model suggests a better prediction in the third stage, which is more relevant in terms of drying time (it represents between 68% and 87% of the drying time), instead of an accurate transition from the second to the

Table 4
Calculated pressures inside the droplet achieved at the end of the second stage when boiling starts.

Formulation	Pressure in the transition from second to third stage (Pa)
A	1.45×10^5
B	1.49×10^5
C	1.8×10^5
D	1.24×10^5
E	1.02×10^5
F	1.42×10^5

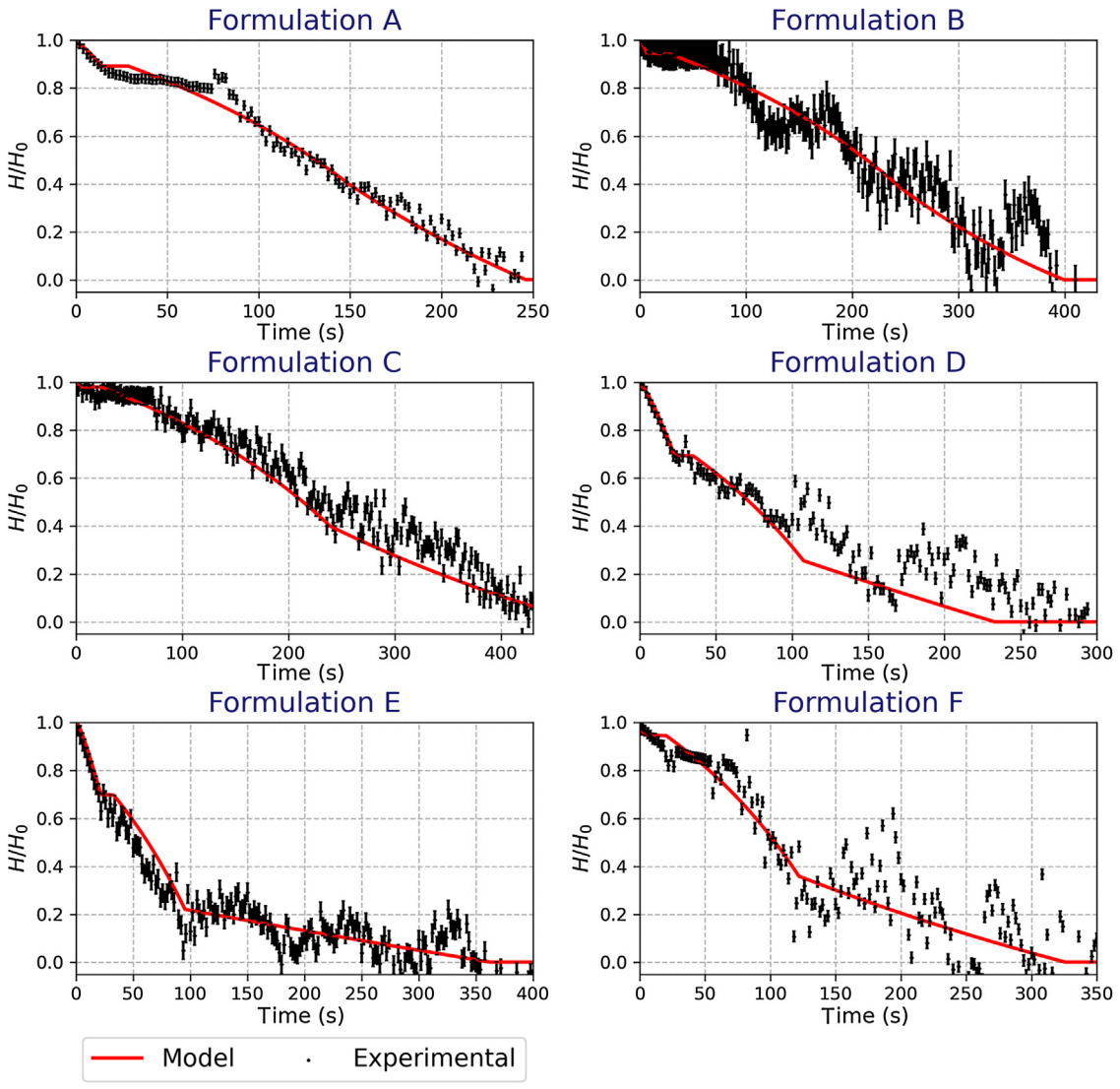

Fig. 5. Experimental data and model predictions of the drying curves for each of the six formulations evaluated in this study (experimental data ., model ——).

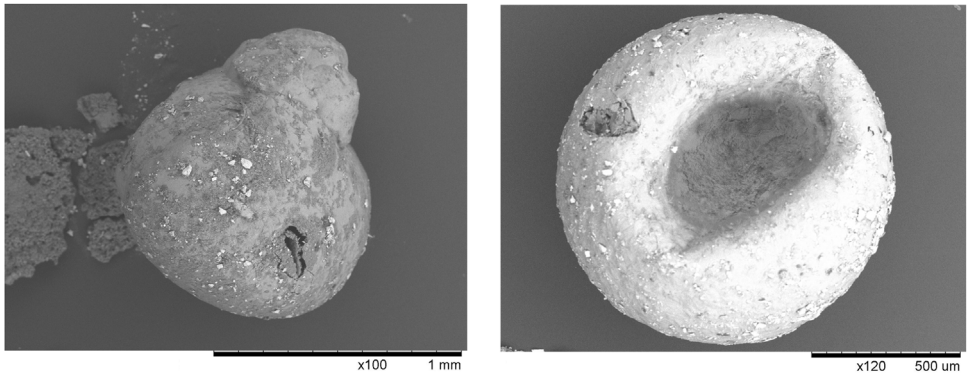

Fig. 6. Final droplet structure observed from SEM analysis for two different formulations.

third stage. This influence in trying to predict accurately the third stage, whose parameters have been estimated with ranges near the ones proposed by Ali et al. (2017), also affects on the characterization of pressure at the end of the second stage and subsequently in the estimation of the porosity. Comparing the tortuosity values obtained from the porosity and the effective diffusion coefficient of the crust following Eq. (27), we obtain values between 4 and 70 for the tortuosity of the different formulations. These values are higher than expected, which can be explained for the complex composition of the detergent and the assumption of taking the diameter of the crust that compose the particles to be 1 μm. This value can be higher since some particles can nucleate forming bigger shapes or in some cases there can also form a film due to the presence of surfactants and plastic compounds that interact each other. To

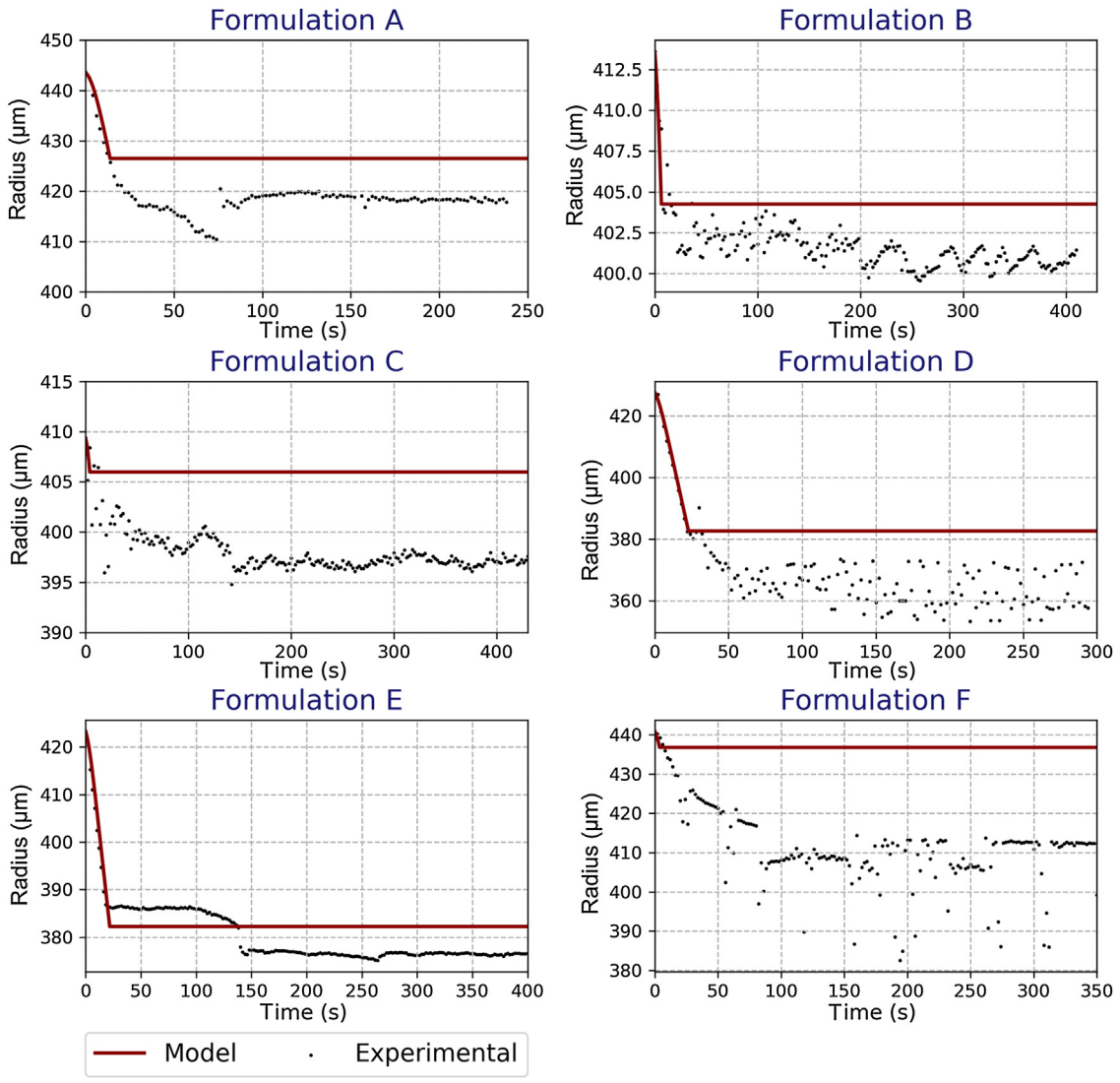

Fig. 7. Experimental data and model predictions of droplet radius for each of the six formulations evaluated in this study (experimental data ·, model —).

understand the role and the possible interaction between the particulate material and the remaining compounds, in future works the particulate material with a characterized particle size needs to be evaluated first with water and then with the remaining compounds of the detergent.

$$\tau = \varepsilon \cdot \frac{D_w}{D_{cr}} \tag{27}$$

The high fraction of time that this third stage represents over the whole drying time can also explain why previous researchers (Ali et al., 2017; Jaskulski et al., 2016) have obtained good results when they validate the SDD model with temperature measurements in the tower. However, comparing with the work of Ali et al. (2017), where a polynomial was used for the modelling of the second stage, the current work provides a physical explanation for the phenomena that generate these stages. It also addresses the fact that higher pressures and temperatures can be achieved within the core at the end of the second stage and that these temperatures are governed by the crust's thickness and the pores that it contains.

Radius evaluation

Fig. 7 presents the validation of the radius profile. It can be seen that the radius is predicted correctly for some formulations but not for formulations A, D and F. The experimental results show an initial decrease in the size due to the evaporation of the moisture in the surface until it gets saturated and the formation of the crust begins. In the second stage, the radius behaves differently for some of the formulations studied. In cases A, D and F, this radius continues to show a slight decrease resulting in a small lack of accuracy in the final prediction of the droplet size. Although this lack of accuracy may cause errors in the evaluation of other phenomena such as drying in boiling conditions, particle density or agglomeration (Jubaer et al., 2017), the average error only reaches 4.8% of the total particle radius in the worst case, formulation D.

Other variables computed by the model

Another variable that can be used for validation of the experiments is the droplet density. This variable is derived from the radius and the particle moisture content. A lack of prediction in either the droplet's radius or its moisture content results in an inaccurate prediction of its density. It is presented in Fig. 8 and the final value is shown to be predicted well for all the formulations except D where the higher radius predicted by the model results in a lower density. There is also an error in predicting the density at the end of the second stage for formulation B, for which a shorter second stage was predicted by the model. However, this lack of accuracy in the prediction of the droplet density is finally corrected during

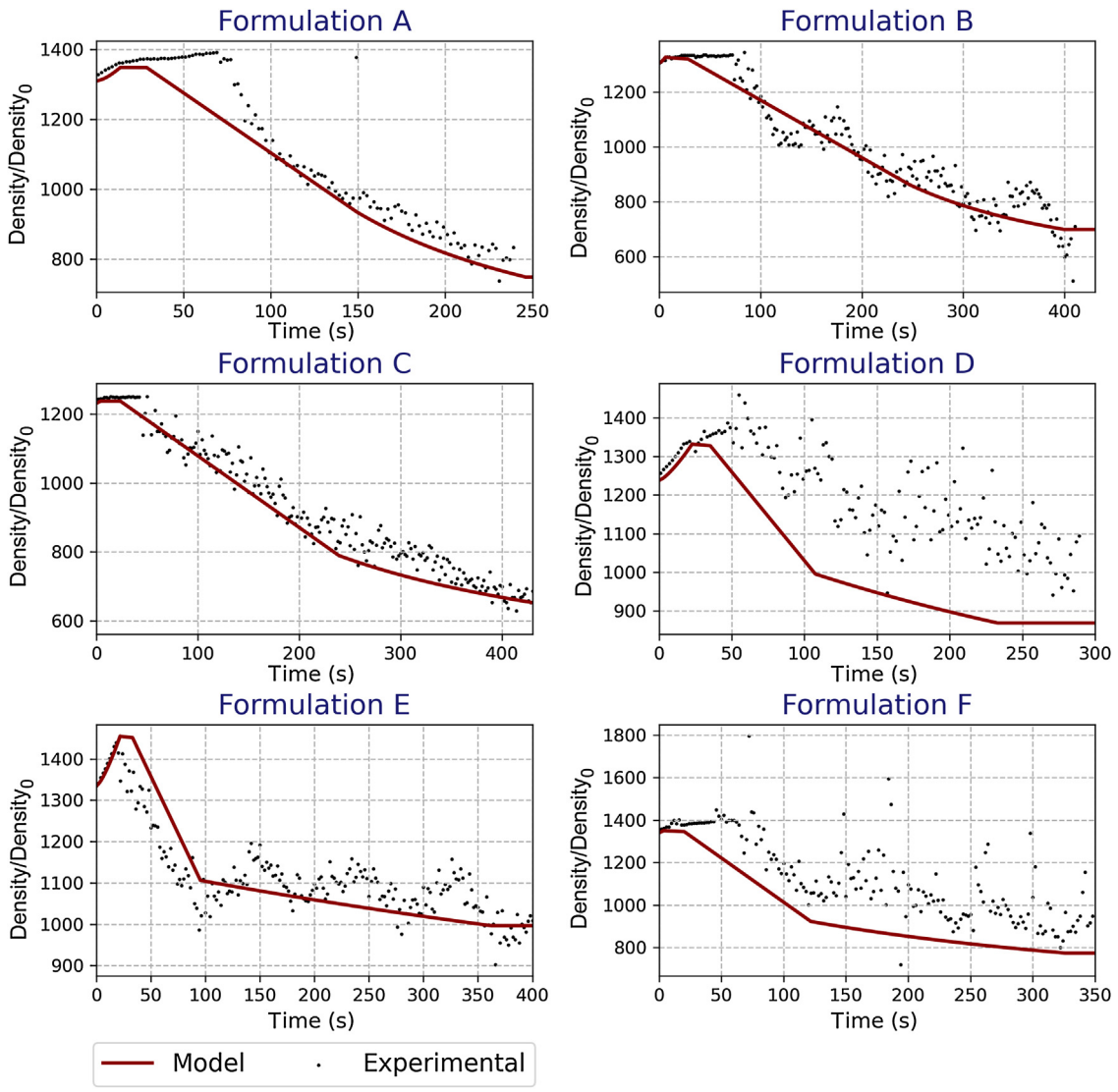

Fig. 8. Experimental data and model predictions of relative droplet density for each of the six formulations evaluated in this study (experimental data ., model ——).

the third stage, which takes most of the total drying time, and the final density of the particle is predicted well.

Another critical variable in SDD is the droplet temperature. The temperature computed by the model is presented in Fig. 9. The method used to measure the SDD of the particles does not provide the particle temperatures and their validation cannot be carried out. However, the use of alternative single droplet drying methods that measure the particle temperature are intrusive and modify the structure of the crust favouring apertures near the thread used for the thermocouple and subsequently a lower boiling temperature than the real one. The only non-intrusive alternative is the use of a thermographic camera. It can allow the determination of the surface temperature (Wulsten & Lee, 2008). However, for the formulations evaluated in this study a crust is formed and such methods do not allow the prediction of the temperature in the wet core of the particle. Therefore, these predictions could not be validated either. Their validation will be more relevant for the third stage where the drying is governed by boiling and the drying rates depends on the boiling temperature reached by the droplet.

Analysing the temperature estimated for the droplets during this third stage, it can be seen that boiling conditions are achieved above the boiling temperature of water at atmospheric conditions. As a result of this higher temperature, the temperature difference between the heat transfer media, the crust, and the core is small and the nucleate boiling regime, where bubbles are generated, is not achieved. The droplet is then in the free convection regime of boiling, see Fig. S3 of the supplementary material. Thus, as presented in Fig. 5 for the experimental humidity of the droplet and the videos attached in the supplementary material, there is no bursting in the droplet. To identify the temperature where this bursting takes place for every formulation, in addition to evaluating the SDD under different temperatures, future work should also study the transition to the bubble nucleation regime. Such a study will help to understand the temperature difference at which stable bubble jets are generated under different concentrations and for every formulation.

Conclusions

In tis work, the drying curves for six different detergent formulations have been presented. The experiments are performed by mean of an acoustic levitator at 393 K. For these experiments, drying appears to take place in three stages:

- A surface drying stage with a shrinkage of the droplet until the surface gets saturated.

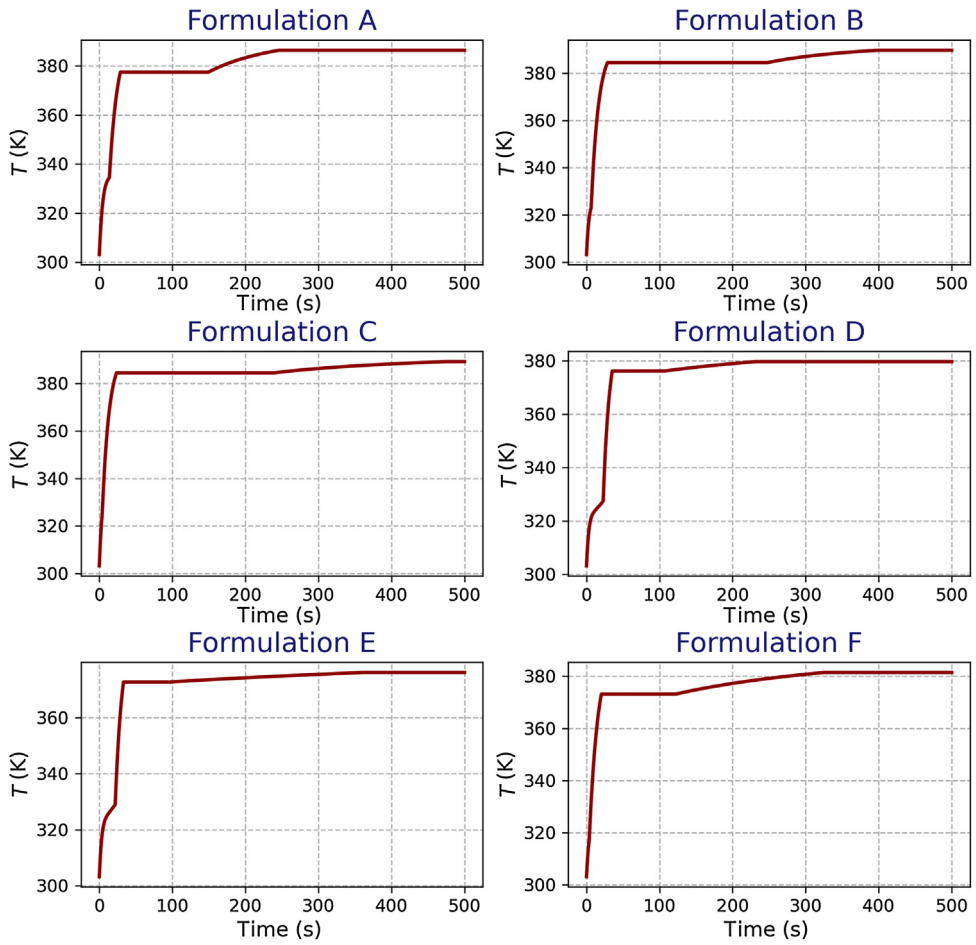

Fig. 9. Temperatures computed by the model.

- A second stage where the where the drying is governed by the diffusive resistance of water through the pores. This stage lasts until boiling conditions are achieved. Since the temperature difference between the bulk and the droplet core is not big enough, stable bubbles are not generated within the core and no bursting is observed in the droplet. Thus, it has been showed that boiling can occur during the drying of the droplet but does not always result in bursting.
- A third stage controlled by boiling temperature until the final equilibrium moisture content is achieved.

To shred light into the drying mechanism, a first principles-based model is proposed. The model has been used to study the SDD experiments described in this work. It is capable of predicting the moisture content for all the formulations studied in this work and is also implementable in CFD codes for the scale-up of drying. Furthermore, this model also provides a physical basis to explain:

First, the controlled drying in the second stage where the pores in the crust govern the drying and it is not exclusively a function of the time until boiling as proposed by Ali et al. (2017). This formation of the crust is not only relevant in terms of drying but it can be also important in the prediction of the agglomerates formed by particle-wall interaction. As shown in the work of Francia, Martín, Bayly, and Simmons (2016) a significant concentration of deposits is obtained at the end of the nozzle where the droplets/particles impact the wall, in some cases at high velocity. These agglomeration regions cannot only be formed by the droplets but also by those particles with high velocity that have a very thin crust that release the water after impact.

Second, the transition to the third stage obtained at pressures higher than atmospheric due to the pressure drop in the crust thickness. This fact must be taken into account if the modified Antoine equation proposed in Eq. (22) is to be applied from the independent characterization of the formulation

In the third stage, two periods are distinguished. In the first period, accumulation of heat within the core does not occur and the temperature in the core is only control by the pressure drop through the pores. In the second period, the temperature in the core increases partly due to an increase in the concentration of the solids and partly because higher pressures are necessary to achieve the equilibrium in the core.

Conflicts of interest

None declared.

Declaration of Competing Interest

The authors report no declarations of interest.

Acknowledgements

The authors gratefully acknowledge Procter & Gamble for financial support and financial support from Universitat Jaume I and Fundació Caixa Castelló-Bancaixa (projects: P11B2006-37 and P11B2009-27).

Appendix A. Supplementary data

Supplementary material related to this article can be found, in the online version, at https://doi.org/10.1016/j.partic.2021.01.012.

References

Abramzon, B., & Sirignano, W. A. (1989). Droplet vaporization model for spray combustion calculations. *International Journal of Heat and Mass Transfer*, *32*, 1605–1618.

Adhikari, B., Howes, T., Bhandari, B. R., & Troung, V. (2003). Surface stickiness of drops of carbohydrate and organic acid solutions during convective drying: Experiments and modelling. *Drying Technology*, *21*, 839–873.

Ali, M., Mahmud, T., Heggs, P. J., Ghadiri, M., Bayly, A. E., Ahmadian, H., et al. (2017). CFD modelling of a pilot-scale counter-current spray drying tower for the manufacture of detergent powder. *Drying Technology*, *35*(3), 281–299.

Chen, X. D., Farid, M., Reid, D., Fletcher, A., Pearce, D., & Chen, N. X. (1997). A new model for the drying of milk droplets for fast computation purposes. In R. S. Jebson, R. Chong, & M. Ozilgen (Eds.), *Proceedings Chemeca'97* (pp. 825–830).

Chen, X. D., & Putranto, A. (2013). *Modeling drying processes: A reaction engineering approach*. Cambridge: Cambridge University Press. ISBN: 9781107012103

Chen, X. D., & Xie, G. Z. (1997). Fingerprints of the drying behaviour of particulate or thin layer food materials established using a reaction engineering model. *Transactions of the Institution of Chemical Engineers C*, *75*, 213–222.

Dannenberg, F., & Kessler, H. (1988). Reaction kinetics of the denaturation of whey proteins in milk. *Journal of Food Science*, *53*(1), 258–263.

Darvan, A., & Sommerfeld, M. (2014). Modeling and numerical analysis of the drying stages during single droplet drying. *19th international drying symposium, IDS 2014*.

Ebrahim, W. A. M. (2019). *Single droplet drying at high temperatures*. University of Leeds. PhD thesis.

Farid, M. M. (2003). A new approach to modelling of single droplet drying. *Chemical Engineering Science*, *58*, 2985–2993.

Francia, V., Martín, L., Bayly, A. E., & Simmons, M. J. H. (2016). Agglomeration in counter-current spray drying towers. Part A: Particle growth and the effect of nozzle height. *Powder Technology*, *301*, 1330–1343.

Griffith, J. D., Bayly, A. E., & Johns, M. L. (2008). Magnetic resonance studies of detergent drop drying. *Chemical Engineering Science*, *63*, 3449–3456.

Groenewold, C., Möser, C., Groenewold, H., & Tsotsas, E. (2002). Determination of single-particle drying kinetics in an acoustic levitator. *Chemical Engineering Journal*, *86*, 217–222.

Handscomb, C. S., Kraft, M., & Bayly, A. E. (2009). A new model for the drying of droplets containing suspended solids after shell formation. *Chemical Engineering Science 2009*, *64*(2), 228–246.

Harvie, D. J. E., Langrish, T. A. G., & Fletcher, D. F. (2002). A computational fluid dynamics study of a tall-form spray dryer. *Food and Bioproducts Processing*, *80*, 163–175.

Hecht, J. P., & King, C. J. (2000). Spray drying: Influence of developing drop morphology on drying rates and retention of volatile substances. 2. Modeling. *Industrial & Engineering Chemistry Research*, *39*, 1766–1774.

Hernández, B., Fraser, B., Martin de Juan, L., & Martin, M. (2018). Computational fluid dynamics (CFD) modeling of swirling flows in industrial counter-current spray drying towers under fouling conditions. *Industrial & Engineering Chemistry Research*, *57*(35), 11988–12002.

Incropera, F. P., Dewitt, D. P., & Bergman, T. L. (2006). *Fundamentals of heat and mass transfer* (6th Ed.). ISBN: 978-0-471-45728-2.

Jaskulski, M., Zbicinski, I., & Wawrzyniak, P. (2015). CFD simulation of particle agglomeration in industrial counter-current spray drying tower. *Presented at the 1st Nordic Baltic drying conference*, 2015.

Jaskulski, M., Wawrzyniak, P., & Zbicinski, I. (2016). CFD prediction of powder particle size distribution in the industrial scale spray drying process. *20th international drying symposium (IDS 2016) Gifu*.

Jubaer, H., Afshar, S., Xiao, J., Chen, X. D., Selomulya, C., & Woo, M. W. (2017). On the importance of droplet shrinkage in CFD modelling of spray drying. *Drying Technology*, *36*, 1785–1801.

Keey, R. B., & Suzuki, M. (1974). On the characteristic drying curve. *International Journal of Heat and Mass Transfer*, *17*, 1455–1464.

Langrish, T. A. G. (2009). Multi-scale mathematical modelling of spray dryers. *Journal of Food Engineering*, *93*, 218–228.

Langrish, T. A. G., & Kockel, T. K. (2001). The assessment of a characteristic drying curve for milk powder for use in computational fluid dynamics modelling. *Chemical Engineering Journal*, *84*, 69–74.

Lin, S. X. Q., & Chen, X. D. (2002). Improving the glass-filament method for accurate measurement of drying kinetics of liquid droplets. *Chemical Engineering Research and Design*, *80, 4*, 401–410.

Lin, S. X., & Chen, X. D. (2005). Air drying of milk droplet under constant and time-dependent conditions. *AIChE Journal*, *51*(6), 1790–1799.

Liou, J. K., & Bruin, S. (1981). An approximate method for the nonlinear diffusion problem with a power relation between diffusion coefficient and concentration – I. *Computation of Desorption Times*.

Kastner, O., Brenn, G., Rensink, D., & Tropea, C. (2000). Mass transfer from multiphase droplets during drying in a tube levitator. *Proceedings of the 8th international conference on liquid atomization and spray systems*.

Keey, R. B. (1992). *Drying of loose and particulate materials*. New York, 1992: Hemisphere Publishing.

Kieviet, F. G. (1997). *Modelling quality in spray drying. PhD. Thesis*. The Netherlands: T.U. Eindhoven.

Koniorczyk, M., & Konca, P. (2013). Experimental and numerical investigation of sodium sulphate crystallization in porous materials. *Heat and Mass Transfer*, *49*, 437–449.

Masters, K. (1992). *Spray drying handbook* (5th Ed.). UK: Longman Scientific and Technical.

Mezhericher, M., Levy, A., & Borde, I. (2008). Modelling of particle breakage during drying. *Chemical Engineering and Processing*, *47*, 1404–1411.

Mezhericher, M., Levy, A., & Borde, I. (2010). Theoretical models of single droplet drying kinetics: A review. *Drying Technology*, *28*(2), 278–293.

Mezhericher, M., Naumann, M., Peglow, M., Levy, A., Tsotsas, E., & Borde, I. (2012). Continuous species transport and population balance models for first drying stage of nanosuspension droplets. *Chemical Engineering Journal*, *210*, 120–135.

Minoshima, H., Matsushima, K., Liang, H., & Shinohara, K. (2002). Estimation of diameter of granule prepared by spray drying of slurry with fast and easy evaporation. *Journal of Chemical Engineering of Japan*, *35*, 880–885.

Mondragon, R., Hernandez, L., Enrique Julia, J., Jarque, J. C., Chiva, S., Zaitone, B., et al. (2011). Study of the drying behaviour of high load multiphase droplets in an acoustic levitator at high temperature conditions. *Chemical Engineering Science*, *66*, 2734–2744.

Mujumdar, A. S., & Huang, L. X. (2007). Global R&D needs in drying. *Drying Technology*, *25*(4), 647–658.

Nesic, S., & Vodnik, J. (1991). Kinetics of droplet evaporation. *Chemical Engineering Science*, *46*(2), 527–537.

Patel, K. C., Chen, X. D., Lin, S. X. Q., & Adhikari, B. (2009). A composite reaction engineering approach to drying of aqueous droplets containing sucrose, maltodextrin (DE6) and their mixture. *AIChE Journal*, *55*(1), 217–231.

Ranz, W. E., & Marshall, W. R. (1952a). Evaporation from drops part 1. *Chemical Engineering Progress*, *48*(3), 141–146.

Ranz, W. E., & Marshall, W. R. (1952b). Evaporation from drops part 2. *Chemical Engineering Progress*, *48*(4), 173–180.

Sano, Y., & Keey, R. B. (1982). The drying of a spherical particle containing colloidal material into a hollow sphere. *Chemical Engineering Science*, *37*(6), 881–889.

Seydel, P., Sengespeick, A., Blomer, J., & Bertling, J. (2004). Experiment and mathematical modelling of solid formation at spray drying. *Chemical Engineering Technology*, *27*(5), 505–510.

Seydel, P., Blomer, J., & Bertling, J. (2004). Experiment and mathematical modelling of solid formation at spray drying. *Chemical Engineering and Technology*, *27*(5), 505–510.

Strumillo, C., & Kudra, T. (1986). *Drying: Principle. Application and design*. pp. 45–54. New York: Gordon and Breach.

Tsotsas, E., & Mujumdar, A. S. (2009). *Modern drying techonology. Volume 2: Experimental techniques*. Wiley-VCH Verlag GmbH & Co. ISBN: 978-3-527-31557-4.

Tran, T. T. H., Jaskulski, M., Avila-Acevedo, J. G., & Tsotsas, E. (2017). Model parameters for single-droplet drying of skim milk and its constituents at moderate and elevated temperatures. *Drying Technology*, *35*, 444–464.

Woo, M. W. (2017). *Computational fluid dynamics simulation of spray dryers. An engineer's guide*. Taylor & Francis Group:Boca Raton, FL: CRC Press. ISBN: 978-1-4987-2464-7.

Woo, M. W., Daud, M. R. W., Mujumdar, A. S., Talib, M. Z. M., Hua, W. Z., & Tasirin, S. T. (2008). Comparative study of droplet drying models for CFD modelling. *Chemical Engineering Research and Design*, *86*, 1038–1048.

Wulsten, E., & Lee, G. (2008). Surface temperature of acoustically levitated water microdroplets measured using infra-red thermography. *Chemical Engineering Science*, *63*, 5420–5424.

Yarin, A. L., Brenn, B., Kastner, O., Rensink, D., & Tropea, C. (1999). Evaporation of acoustically levitated droplets. *Journal of Fluid Mechanics*, *399*, 151–204.

Yarin, A. L., Brenn, G., Kastner, O., & Tropea, C. (2002). Drying of acoustically levitated droplets of liquid-solid suspensions: Evaporation and crust formation. *Physics of Fluids*, *14*, 2289. https://doi.org/10.1063/1.1483308

Zbicinski, I. (2017). Modeling and scaling up of industrial spray dryers: A review. *Journal of Chemical Engineering of Japan*, https://doi.org/10.1252/jcej.16we350

Zbicinski, I., & Li, X. (2006). Conditions for accurate CFD modeling of spray-drying process. *Drying Technology*, *24*, 1109–1114.